Nuclear shape evolution of neutron-deficient Au and kink structure of Pb isotopes

Myeong-Hwan Mun [1], Eunja Ha,[2] Yong-Beom Choi,[3] and Myung-Ki Cheoun [1,*]

[1]*Department of Physics and Origin of Matter and Evolution of Galaxies (OMEG) Institute, Soongsil University, Seoul 06978, Korea*
[2]*Department of Physics and Research Institute for Natural Science, Hanyang University, Seoul 04763, Korea*
[3]*Center for Innovative Physicist Education and Research, Pusan National University, Busan 46241, Korea*

Recent experiments using advanced laser spectroscopy technique revealed that the charge radii of neutron-deficient gold (Au) isotopes exhibit significant changes in ground state deformation: odd-even shape staggering in the $N = 98$–100 region and abrupt change of charge radii from $N = 108$. In this study, we examine the abnormal evolution of the nuclear charge radii. To understand the nuclear structure underlying this phenomenon, we exploit the deformed relativistic Hartree-Bogoliubov theory in continuum (DRHBc). The significant change in mean-squared charge radii ($\delta \langle r^2 \rangle$) turns out to originate from nuclear shape transitions between prolate deformation and small oblate deformation due to the shape coexistence possibility. We elucidate the nuclear shape evolution by analyzing the evolution of occupation probability for single-particle states. In addition, the abrupt kink structure in the nuclear charge radius of lead (Pb) isotopes near the $N = 126$ shell is also investigated and reproduced quite well.

I. INTRODUCTION

The nuclear charge radius is one of the most important properties that can be direct evidences of the fundamental characteristics of nuclear structure. Furthermore, it is significant in investigating the evolution of nuclear structures, including the emergence of new magic numbers or the disappearance of traditional magic numbers [1–4]. In particular, the nuclear charge radius could provide critical information for shape transition and coexistence [5–9] as well as isomerism [10–12].

If a constant saturation density is assumed inside the nucleus, the nuclear charge radius is typically described by the $A^{1/3}$ law [13–18] or $Z^{1/3}$ law [19], where A and Z are the mass and charge numbers, respectively. In recent years, with the remarkable development of experimental technology, the relative root-mean-square (rms) charge radii of unstable nuclei have been increasingly measured by various approaches such as ion guide isotope separator [20,21], K_α x-ray isotope shifts [22–26], and high-resolution laser spectroscopy [27–35]. These measurements of the hyperfine interaction have been performed on a variety of isotopes, ranging from K and Ca to Au, Pb, and Bi isotopes [4,30,35–47]. Experimental investigations of nuclear charge radii have found meaningful regular patterns, abrupt changes, and nonlinear trends along isotopic chains in the nuclear chart. Most recently, the strong odd-even shape staggering (OES) in some isotopic chains and the abrupt kinks across neutron shell closures have been observed and have attracted lots of interests [32–34,39–41,48–51].

A more accurate description of nuclear charge radii, which are closely associated with nuclear deformation, is necessary for understanding these nuclear shape transitions. In theory, a variety of methods, such as local-relationship-based models [52,53], macroscopic-microscopic models [54,55], nonrelativistic mean-field models [56,57], relativistic mean-field models [58–60], and *ab initio* no-core shell models [61,62] are employed for systematic investigation of nuclear charge radii. Recently, on account of the development of high-performance computing, several machine learning approaches are also widely used to improve the description of nuclear charge radii [63–66]. Although each model provides fairly good descriptions of the nuclear charge radii across the nuclear chart, only a few of these models can accurately reproduce strong odd-even shape staggering (OES) and abrupt kinks across the neutron shell closure [67,68].

In this paper, we demonstrate that the observed shape transition could be attributed to the shape coexistence of the Au and Pb isotopes using the deformed relativistic Hartree-Bogoliubov theory in continuum (DRHBc) approach [69–71]. First, we present the shape coexistence of Au (Pb) isotopes with a precision of 1 MeV (1.5 MeV) using potential energy curves (PECs). Second, we argue that the odd-even shape staggering of Au isotopes in the $N = 98$–100 region and abrupt change $N = 108$ is closely associated with the shape coexistence. Finally, we affirm that the kink structure above ^{208}Pb [46] is closely related to the increase of neutron radii for Pb isotopes. This article is arranged as follows. A brief description of the DRHBc theory used in the present calculation is presented in Sec. II. Detailed results of Au and Pb isotopes including the nuclear shape transition and the kink structure are provided in Sec. III. Finally, the summary and conclusion are given in Sec. IV.

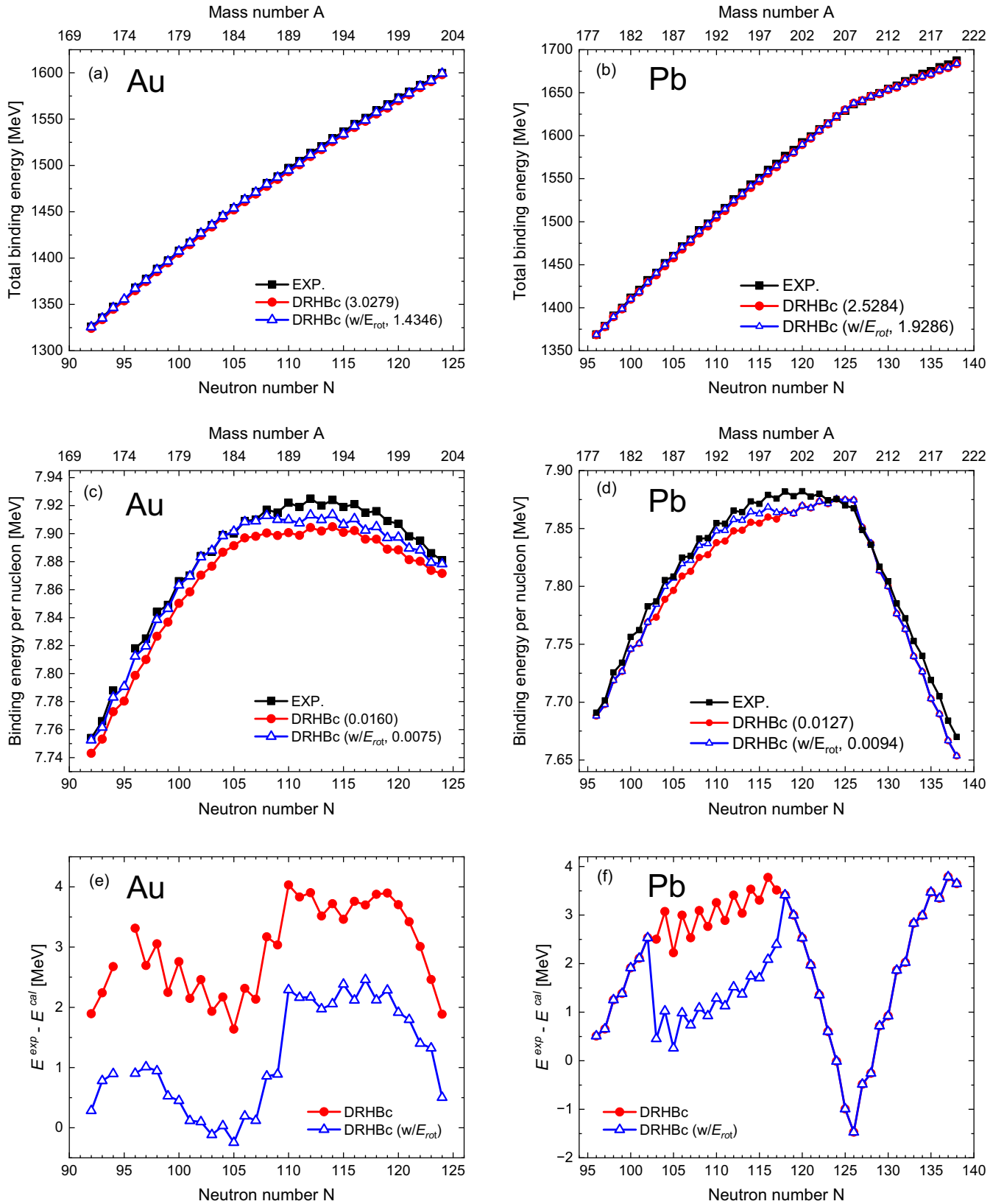---

*Contact author: cheoun@ssu.ac.kr

FIG. 1. TBEs [(a), (b)] and BE/A values [(c), (d)] of Au [Pb] isotopes determined by DRHBc calculations without (red circles) and with (blue triangles) rotational correction E_{rot}. They are compared with available experimental data taken from Ref. [99]. The numbers in parentheses stand for average rms deviation in MeV to the data [99]. The relative difference between the experimental TBE data and the DRHBc calculations are enlarged in the panel (e) and (f), respectively, for Au and Pb isotopes.
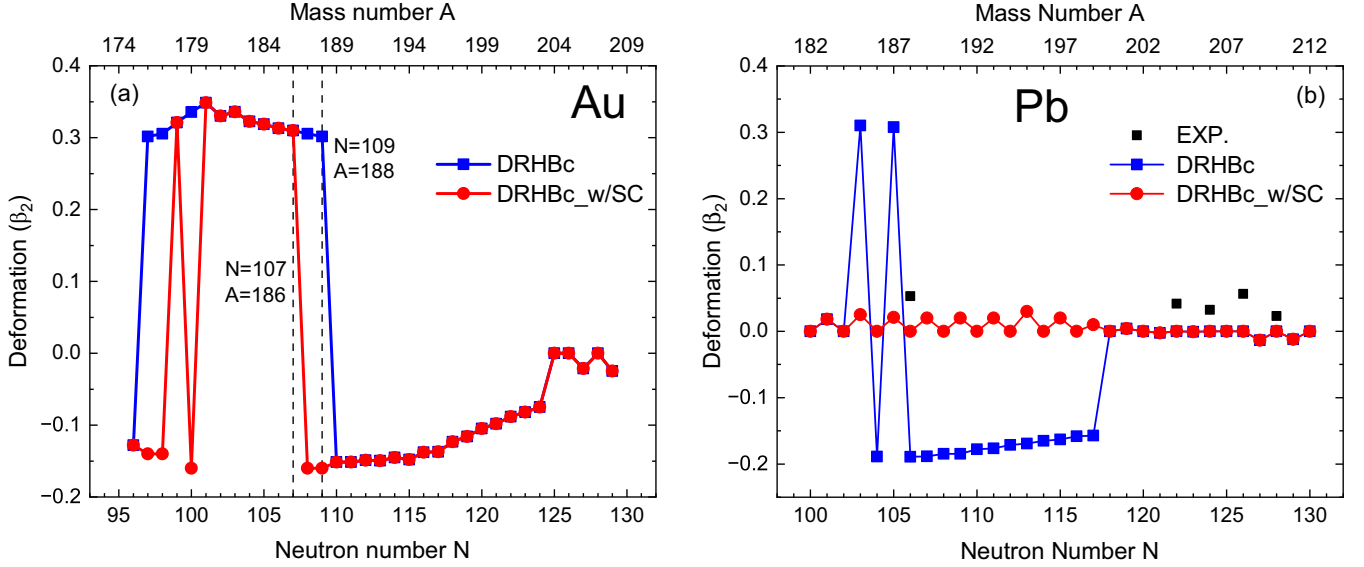
FIG. 2. Quadrupole deformation parameters β_2 of Au (a) and Pb (b) isotopes obtained by DRHBc theory with available experimental data from Ref. [100]. Results shown by blue squares are obtained by DRHBc calculations, while those shown by red circles are obtained by considering the shape coexistence (see the text for details).

II. FORMALISM

In order to comprehensively address the aforementioned issues, a well-refined and state-of-the-art relativistic nuclear model is indispensable. This model should simultaneously consider deformation, pairing correlations, and the continuum effects within a microscopic framework capable of encompassing the entire nuclear mass range. Regarding this issue, the deformed relativistic Hartree-Bogoliubov theory in continuum (DRHBc), based on the meson-exchange [69–71] or point-coupling [72,73] density functional, has been developed. More recently, the DRHBc theory has been successfully extended to deal with odd-mass or odd-odd nuclei by employing an automatic blocking method [73]. The DRHBc theory has been proven to offer a strong description of nuclear masses with high predictive power [58,74–76], and it has demonstrated its capabilities through various applications [77–89]. For example, the DRHBc theory has been successfully applied to shape staggering and kink structure in the Hg isotopes [67], as well as the shape coexistence and prolate dominance in the Te, Xe, and Ba isotopes [90].

In this study, we concentrate on shape coexistence and its subsequent effects, specifically nuclear shape transition, i.e., odd-even shape staggering and abrupt shape change in Au isotopes, and kink structure in Pb isotopes employing the DRHBc theory. The details of the DRHBc theory can be found in Refs. [69–73]. Here, only a brief introduction to the formalism of the DRHBc theory is provided. In the DRHBc theory, the relativistic Hartree-Bogoliubov (RHB) equation [91], which is solved in a Dirac Woods-Saxon basis [92,93], is given as follows:

$$\begin{pmatrix} h_D - \lambda_\tau & \Delta \\ -\Delta^* & -h_D^* + \lambda_\tau \end{pmatrix} \begin{pmatrix} U_k \\ V_k \end{pmatrix} = E_k \begin{pmatrix} U_k \\ V_k \end{pmatrix}, \qquad (1)$$

where λ_τ is the Fermi energy ($\tau = n, p$) for neutrons or protons. E_k and $(U_k, V_k)^T$ are the quasiparticle energy and quasiparticle wave function. In coordinate space, the Dirac Hamiltonian h_D is given by

$$h_D = \boldsymbol{\alpha} \cdot \boldsymbol{p} + V(\boldsymbol{r}) + \beta[M + S(\boldsymbol{r})], \qquad (2)$$

where M is the nucleon mass, and $V(\boldsymbol{r})$ and $S(\boldsymbol{r})$ are the vector and scalar potentials, respectively.

The paring potential Δ is given with the pairing tensor $\kappa(\boldsymbol{r}, \boldsymbol{r}')$ [94] as follows

$$\Delta(\boldsymbol{r}, \boldsymbol{r}') = V(\boldsymbol{r}, \boldsymbol{r}')\kappa(\boldsymbol{r}, \boldsymbol{r}') \qquad (3)$$

with a density-dependent zero range force

$$V(\boldsymbol{r}, \boldsymbol{r}') = \frac{V_0}{2}(1 - P_\sigma)\delta(\boldsymbol{r} - \boldsymbol{r}')\left(1 - \frac{\rho(\boldsymbol{r})}{\rho_{\text{sat}}}\right). \qquad (4)$$

where ρ_{sat} is the nuclear saturation density, V_0 is the pairing strength, and $(1 - P_\sigma)/2$ is the projector for the spin $S = 0$ component in the pairing channel.

For an axially deformed nucleus with spatial reflection symmetry, the potentials and densities can be expanded in terms of Legendre polynomials [95,96],

$$f(\boldsymbol{r}) = \sum_\lambda f_\lambda(r)P_\lambda(\cos\theta), \quad \lambda = 0, 2, 4, \ldots. \qquad (5)$$

To determine the ground state of an odd-mass or odd-odd isotope, consideration should be given to the blocking effect of the unpaired nucleon(s) [94]. For this purpose, the DRHBc theory appropriately handles the blocking effect of unpaired nucleon(s) by employing either the orbital-fixed or automatic blocking procedure in odd nuclei. In the current DRHBc theory, the equal filling approximation [71,97], which preserves time-reversal symmetry and circumvents computationally intensive calculations, is commonly adopted. But we note that the DRHBc theory with time-odd fields strictly
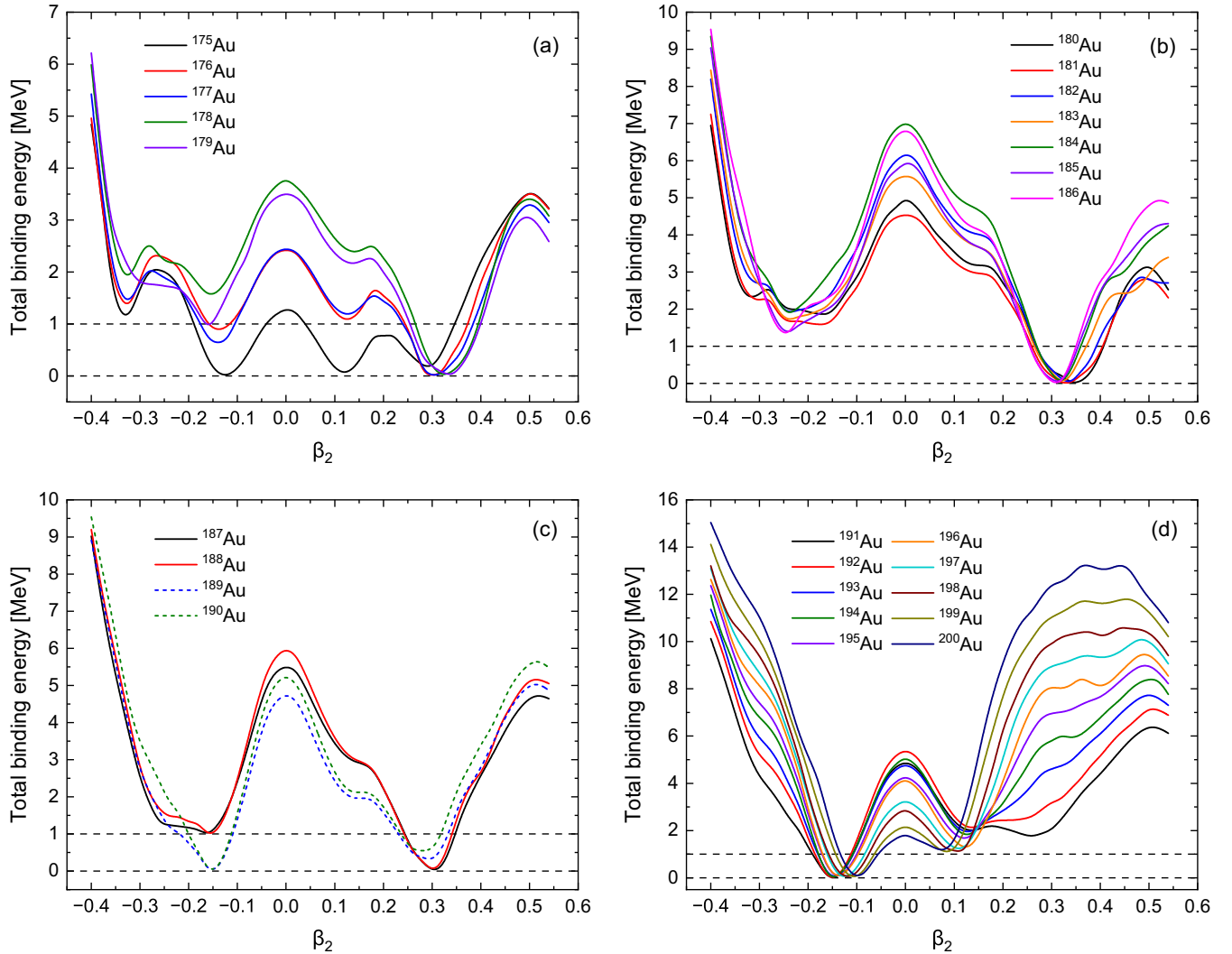
FIG. 3. Evolution of PECs in terms of the deformation parameter β_2 for Au isotopes from the constrained DRHBc calculations. The curves have been scaled to the energy of their ground states. Results of $A = 176$–186 in panels (a) and (b) show the prolate minima corresponding to the results in blue color in Fig. 2(a), while the results of remaining Au isotopes provide oblate deformation. However, the results for $A = 175$–177 and $A = 179$ in panel (a) as well as $A = 187$–190 in panel (c) show the shape coexistence possibility. Detailed PECs for some specific nuclei are presented in Fig. 5.

treated has been developed recently [98]. In Ref. [73], it is confirmed that the DRHBc theory, which incorporates the blocking effect based on the point-coupling functional, is capable of accurately describing odd-mass and odd-odd nuclei. Remarkably, the ground states obtained by the automatic blocking for nuclei such as ^{22}Al and ^{23}Mg were found to be identical to those using the orbital-fixed blocking [73]. This indicates the reliability and consistency of the automatic blocking method in the current numerical calculations.

For the numerical calculations of Au and Pb isotopes, we employ a pairing strength of $V_0 = -325.0$ MeV fm^3, with a pairing window of 100 MeV, and adopt a saturation density of $\rho_{\text{sat}} = 0.152$ fm^{-3}. The energy cutoff $E_{\text{cut}}^+ = 300$ MeV and the angular momentum cutoff $J_{\text{max}} = (23/2)\hbar$ are taken for the Dirac Woods-Saxon basis. In Eq. (5), the Legendre expansion truncation is chosen as $\lambda_{\text{max}} = 8$. The above numerical details

are the same as those used in the global DRHBc mass table calculations over the nuclear chart [72–74].

III. RESULTS

First, we examined the total binding energy (TBE) and binding energy (BE) per nucleon (BE/A) of Au and Pb isotopes by the DRHBc theory. In Fig. 1, the TBEs (a) and BE/A (c) for Au and TBEs (b) and BE/A (d) for Pb obtained from the DRHBc calculations are presented versus the neutron number together with available experimental data [99]. For a quantitative comparison, we provide the difference between the calculated binding energies and the experimental data in Figs. 1(e) and 1(f), which explicitly shows the need of the rotational corrections. Both the TBEs and BE/A demonstrate excellent agreement with the experimental data, showing uncertainties with rms deviation of less than 1.43 MeV and 0.01
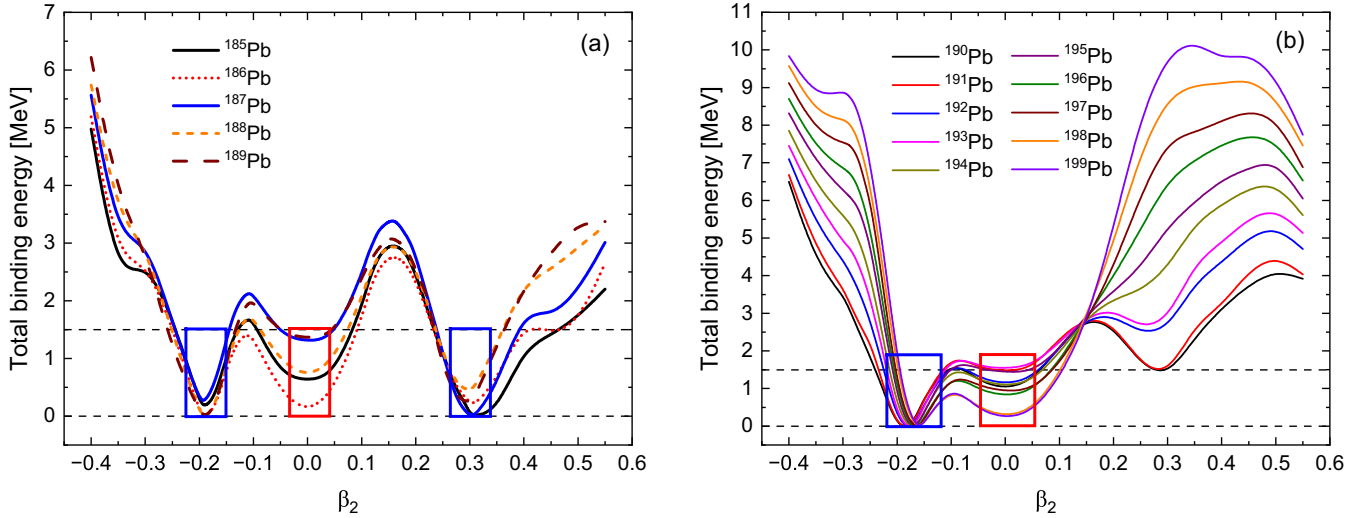
FIG. 4. Evolution of PECs in terms of the deformation parameter β_2 for Pb isotopes from the constrained DRHBc calculations. The curves have been scaled to the energy of their ground states.

MeV (1.93 MeV and 0.01 MeV) in the TBE and BE/A of Au (Pb) by including the rotational correction energy $E_{\rm rot}$. This result serves as a physical guideline for investigating the nuclear shape evolution in the Au isotopes and kink structure in the Pb isotopes. Here we note that the neutron number range is chosen for the region which has the experimental data.

The ground-state quadrupole deformations β_2 calculated by DRHBc are presented in Fig. 2. In all the figure captions, we termed the TBE curves as the potential energy curves (PECs). For gold isotopes [Fig. 2(a)], the prolate deformation is preferred to the oblate deformation in the region $A \leqslant 188$ (see the results of blue squares). The transition from prolate deformations ($\beta_2 < 0.3$) to oblate deformations ($-0.1 < \beta_2 < -0.2$) occurs abruptly at $N = 109$ (^{188}Au). As shown in the blue color results of Fig. 2(b), the majority of lead isotopes within the $185 \leqslant A \leqslant 199$ range (excluding ^{185,187}Pb) favor the oblate deformations ($\beta_2 \simeq -0.2$). Additionally, there is an abrupt transition from oblate deformations ($\beta_2 < -0.2$) to nearly spherical shapes ($\beta_2 \simeq 0$) observed at $N = 118$ (^{200}Pb).

The red circle results are calculated by considering the theoretical shape coexistence, which arises from the competition between the prolate minimum and the oblate minimum for Au isotopes (between the oblate minimum and nearly spherical minimum for Pb isotopes). This is clearly depicted in their PECs in terms of the deformation parameter β_2 for Au (Pb) as shown in Fig. 3 (Fig. 4). We note the local minima in the prolate (oblate) region in the range $175 \leqslant A \leqslant 188$ ($A \geqslant 189$) for Au in Fig. 3 and the local minima in the prolate or oblate (nearly spherical) region in the range $185 \leqslant A \leqslant 199$ ($182 \leqslant A \leqslant 184$ and $A \geqslant 200$) for Pb in Figs. 2 and 4.

To gain a better understanding of the nuclear shape evolution, the detailed PECs for Au and Pb isotopes are presented in Figs. 5 and 6, respectively. The PECs for $^{176-179,187,188}$Au and $^{184-189}$Pb in Figs. 5 and 6 exhibit nearly identical two (three) local minima for Au (Pb) isotopes. This indicates the possibility for shape coexistence, which has been extensively discussed in both theoretical nuclear models and experimental studies over the past few decades [77,101–107]. However, it is

important to note that, for ^{178}Au, the difference of TBE values in the oblate deformation (violet circles) is slightly larger than those of other isotopes (blue circles). This observation offers significant insights for the ensuing discussion on the charge radii evolution in the Au isotopes [35,108–110].

Hereafter, we discuss the charge radii evolution for Au and Pb isotopes. Figure 7 illustrates the experimental data, which reveal the odd-even shape staggering in the $N = 98$–100 region and the sudden change of charge radii above $N = 108$. Theoretical results are obtained by calculating relative changes in mean square charge radii, $\delta \langle r^2 \rangle^{A,A'} = \langle r^2(A) \rangle - \langle r^2(A') \rangle = r_{\rm ch}^2(A) - r_{\rm ch}^2(A')$, with respect to the $A' = 197$ for Au and 208 for Pb, respectively. The results by blue triangles obtained by prolate (oblate) deformations for $A \leqslant 186$ ($A > 188$) for Au isotopes show good agreement with the experimental data (black squares), in Fig. 7(a). However, for ^{176,177,179,187,188}Au, the prolate deformation results (blue triangles) overestimate $\delta \langle r^2 \rangle$. That is, the blue triangles indicating prolate deformation of ^{176,177,179,187,188}Au isotopes are insufficient in explaining the experimental data. But, if we take into account the presence of shape coexistence, the results shown by the red circles obtained using the oblate deformation—the blue circles in Fig. 5—reasonably describe the relative charge radii data within $\delta \langle r^2 \rangle \leqslant 0.25$ fm^2. Indeed, the abrupt change and the observed shape staggering in the Au isotopes is attributed to the transition from oblate deformation to prolate deformation due to the presence of shape coexistence in the Au isotopes, as seen in Figs. 2 and 5. Ultimately, we have successfully reproduced the main features of the experimental results: (i) moving from heavier to lighter masses, the $\delta \langle r^2 \rangle$ value increases significantly at $A = 186$ and (ii) the odd-even shape staggering of charge radii is clearly visible for ^{178}Au isotopes, where the radii for odd-N isotopes are larger than those for neighboring even-N isotopes.

Next, we examine the relative charge radii of Pb isotopes. Figure 7(b) illustrates the evolution of the $\delta \langle r^2 \rangle^{A,208}$ values in
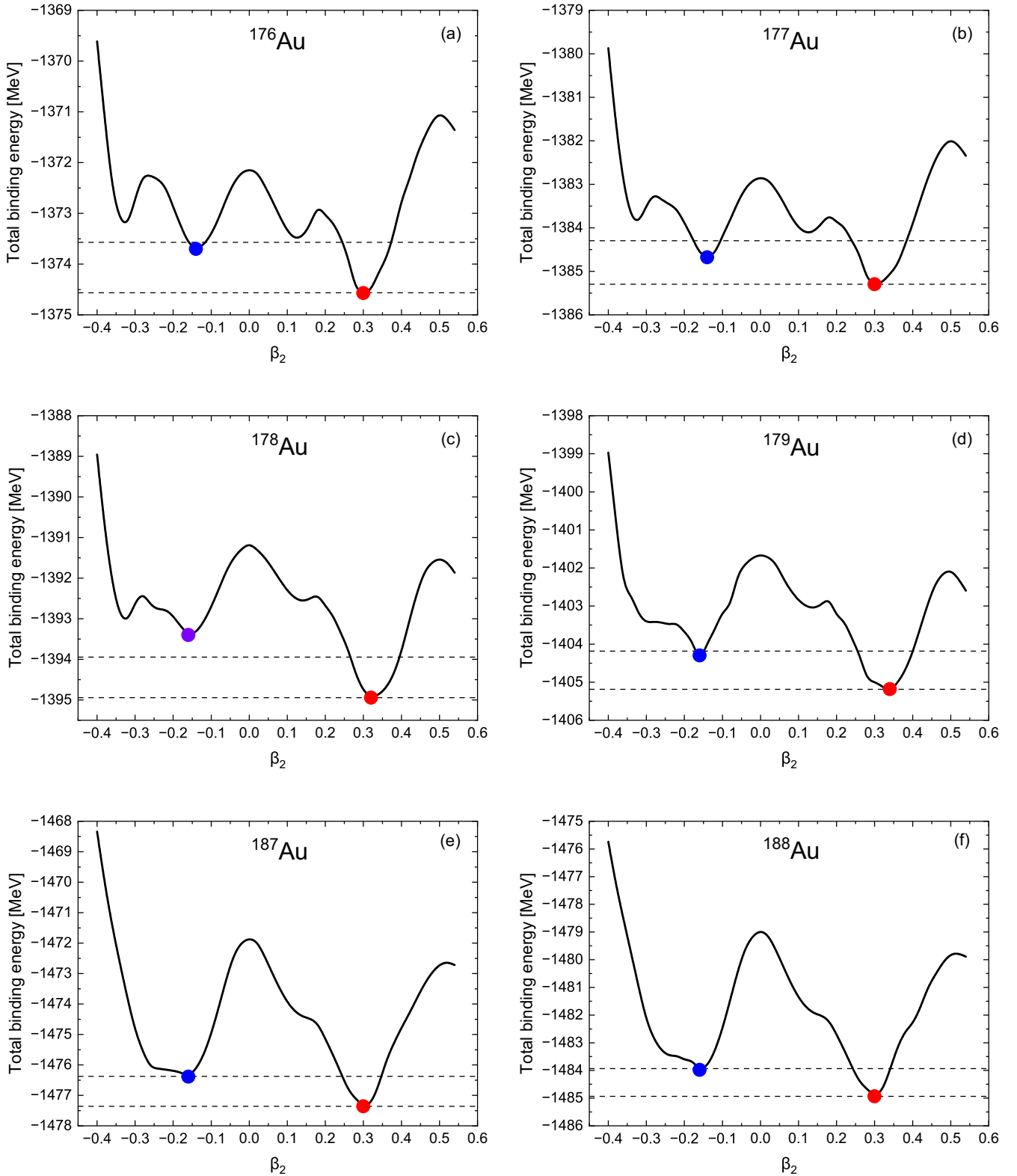
FIG. 5. Detailed PECs in terms of the deformation parameter β_2 for $^{176-179}$Au and ^{187,188}Au isotopes. All of the isotopes demonstrate a possibility of the shape coexistence coming from about 1 MeV energy difference between prolate and oblate minima. But, the violet point in the oblate region in the panel (c) for ^{178}Au is located a bit higher than 1 MeV compared to the prolate deformation.
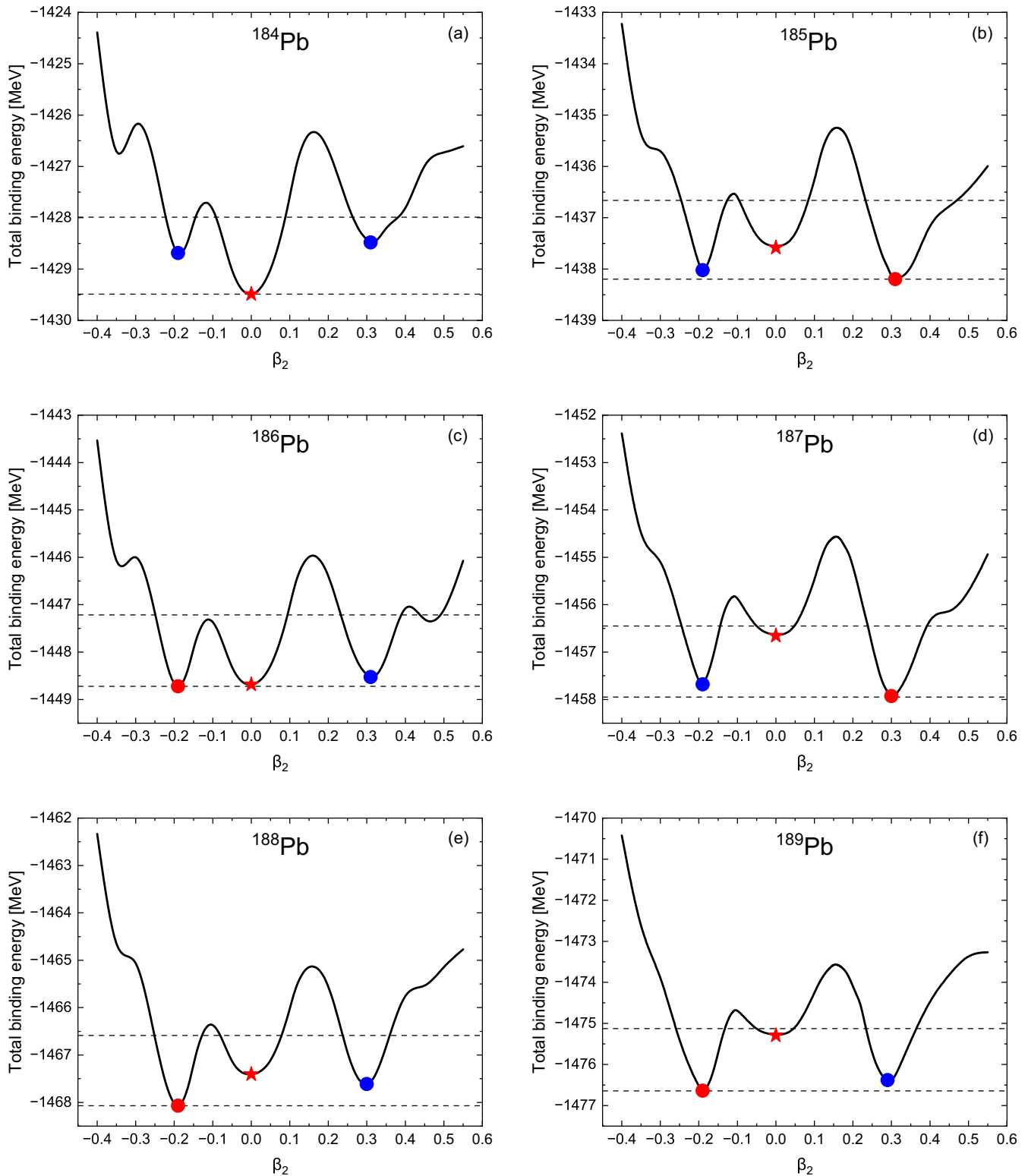
FIG. 6. Detailed PECs in terms of the deformation parameter β_2 for $^{184-189}$Pb isotopes. All of the isotopes demonstrate a possibility of the shape coexistence coming from about 1.5 MeV energy difference among three deformations.

the Pb isotopes. In the region where the neutron numbers $N \geqslant$ 118, the relative charge radii of Pb isotopes are reasonably well reproduced. However, for neutron-deficient Pb isotopes within the range of $100 \leqslant N \leqslant 117$, the relative charge radii

in theoretical results [58,60] are somewhat larger as compared with experiment.

As mentioned in Ref. [58], this overestimation can be attributed to their ground states being predicted a large
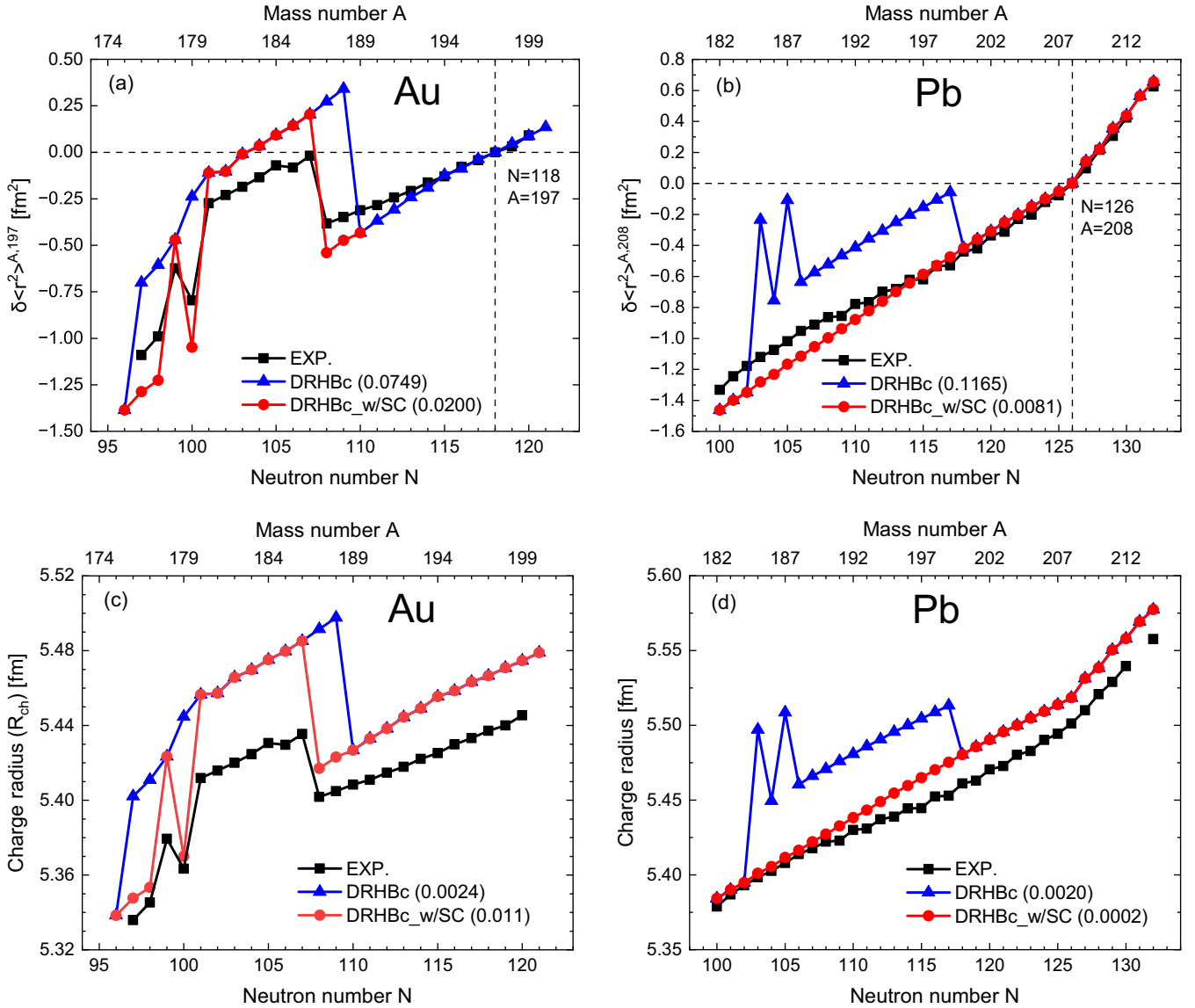
FIG. 7. The relative changes of mean square charge radii $\delta\langle r^2\rangle^{A,197}$ [$\delta\langle r^2\rangle^{A,208}$] [(a), (c)] and charge radii [(c), (d)] for Au isotopes with $N = 96$–121 [for Pb isotopes with $N = 100$–132]. For Au, the results denoted in blue triangles are obtained by prolate shapes calculated by the DRHBc theory and red circles in the region are calculated by oblate deformation considering the shape coexistence presented in Figs. 3 and 5. Considering the shape coexistence, the odd-even shape staggering of charge radii and the abrupt change of charge radii are clearly visible for ^{178}Au isotope and provides a reasonable description. For Pb ($100 \leqslant N \leqslant 117$), the red data result from the spherical shape coexistence. Black boxes for relative changes of mean square charge radii of Au and Pb are taken from experimental data [7,35,108–111]. The numbers in parentheses stand for average rms deviation to the experimental data.

quadrupole deformation, which contradicts experimental observations [112]. Upon examination the experimental charge radii in this neutron range maintain the trend in the $N = 118$–126 region (see Fig. 7(a) in Ref. [60]). In other words, this indicates that the shapes of the nuclei in the measured states are either spherical or nearly spherical. Indeed, if we consider spherical solutions in these nuclei, then the experimental data are rather well reproduced.

However, our calculations using the DRHBc approach predict either oblate or prolate shapes for the ground states of the $N = 103$–117 isotopes [see Fig. 2(b)]. Despite that, spherical minima exist in all isotopes, either close in

energy to the ground states or at some higher energy ($|E| \leqslant 1.5$ MeV), as shown in Figs. 4 and 6. Therefore, considering shape coexistence similarly to the case of Au, the results [red circles in Fig. 7(b)] for Pb obtained by spherical deformation corresponding to the red square of Fig. 4 (and the red star in Fig. 6) provide a reasonable description of the relative charge radii data within $\delta\langle r^2\rangle \leqslant 0.2$ fm^2.

The results of charge radii for Au and Pb isotopes in Figs. 7(c) and 7(d) exhibit a pattern similar to the relative changes of mean square charge radii observed, respectively, in Figs. 7(a) and 7(b).
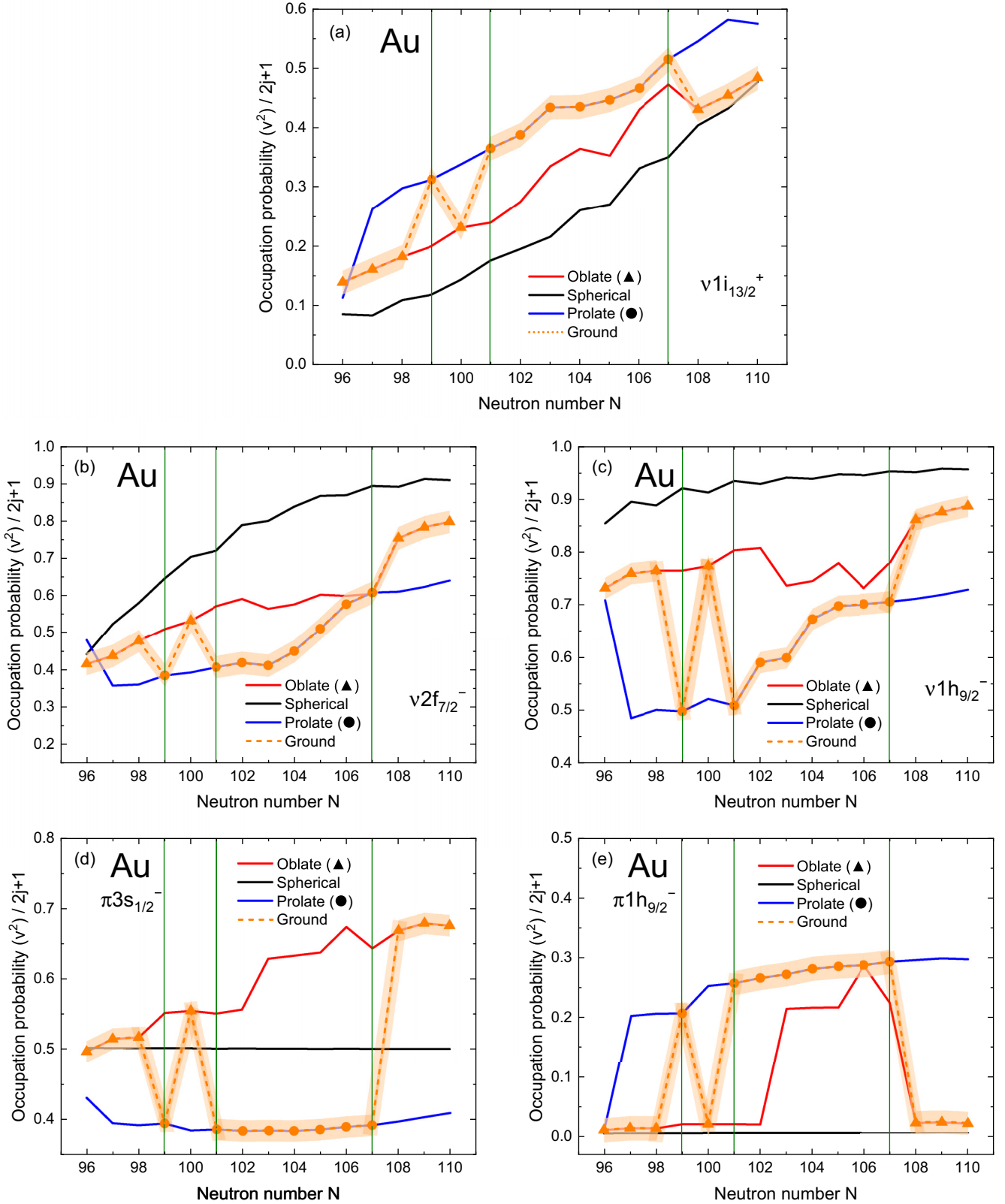
FIG. 8. Evolution of occupation probabilities of the neutron $\nu 1i_{13/2}$ (a), $\nu 2f_{7/2}$ (b), and $\nu 1h_{9/2}$ (c) SPSs and of proton $\pi 3s_{1/2}$ (d) and $\pi 1h_{9/2}$ (e) SPSs for the Au isotopes. In the prolate deformation region, the occupation probabilities of $\nu 1h_{9/2}$, $\nu 2f_{7/2}$, and $\pi 3s_{1/2}$ states decrease while those of $\nu 1i_{13/2}$ and $\pi 1h_{9/2}$ states increase compared to the spherical one. The shaded regions indicate the ground state considering the shape coexistence.
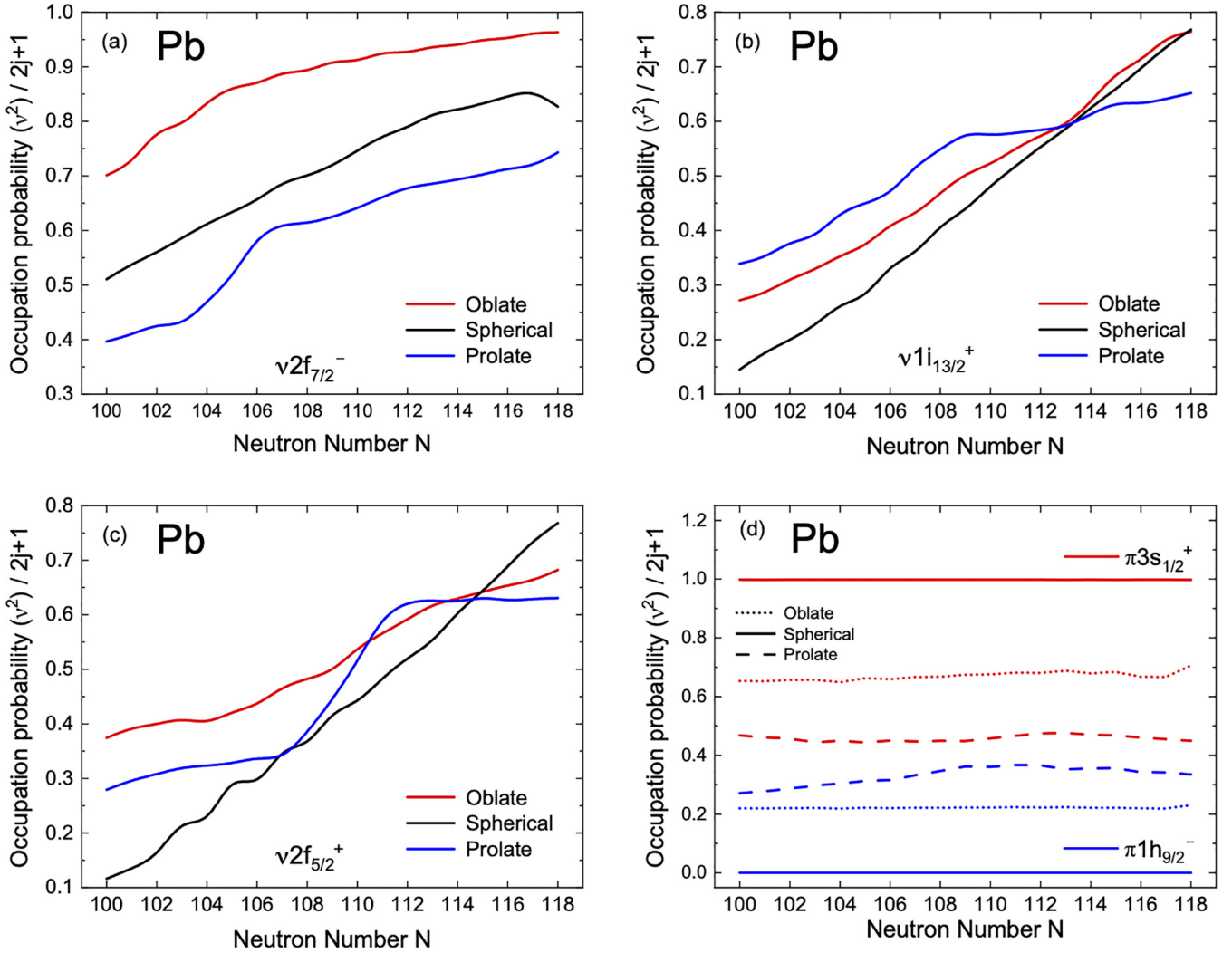
FIG. 9. Evolution of occupation probabilities of the neutron $\nu 2f_{7/2}$ (a), $\nu 1i_{13/2}$ (b), and $\nu 2f_{5/2}$ (c) SPSs and of proton $\pi 3s_{1/2}$ and $\pi 1h_{9/2}$ (d) SPSs for the Pb isotopes. The occupation probabilities of the neutron (a), (b), and (c) SPSs for Pb isotopes are almost monotonically increased with the increase of neutron number, but those of proton (d) SPSs are unchanged.

In Fig. 8, the evolution of occupation probabilities for neutron single-particle states (SPSs), including $\nu 1i_{13/2}$, $\nu 2f_{7/2}$, and $\nu 1h_{9/2}$, as well as proton SPSs, such as $\pi 3s_{1/2}$ and $\pi 1h_{9/2}$, are depicted for Au. We specifically focused on the the occupation probability of the $\nu 1i_{13/2}$ state, as noted in Ref. [30]. The triangles and circles represent the oblate and prolate deformations for Au isotopes, respectively. Remarkably, in Fig. 8(a), one can see that the pronounced increase in the occupation probability of the $\nu 1i_{13/2}$ state explicitly manifests in the prolate deformed ^{178,180,186}Au isotopes. Conversely, in Figs. 8(b) and 8(c), we also observe a decrease in the occupation probability of the $\nu 1h_{9/2}$ and $\nu 2f_{7/2}$ states, which compensates for the abrupt change in the occupation probability of the $\nu 1i_{13/2}$ state. Similarly, in Figs. 8(d) and 8(e), we notice comparable patterns in the proton occupation probabilities for $\pi 3s_{1/2}$ (decrease) and $\pi 1h_{9/2}$ (increase) states for the three Au isotopes. As mentioned in the previous paper [67], this implies that the $\pi 1h_{9/2}$ state plays a key role in the abrupt increase of the charge radii of the Au isotopes. These surges can be attributed not only to the quadrupole

constituent of the nucleon-nucleon interaction but also to the monopole interaction between the $\nu 1i_{13/2}$ state and the $\nu 1h_{9/2}$ state [30]. However, for Pb isotopes, the occupancy probabilities of neutron SPSs increase, while proton SPSs for Pb isotopes are unchanged, as shown in Fig. 9. It means that the shape staggering of Au isotopes comes from the shape transitions of neutron and proton SPSs while the increase of charge radii of Pb isotopes is due to the increase of neutron numbers, implying no discernible change of the symmetric core part composed by $Z = 82$ protons. Here we note that the quantum states of the SPSs of protons and neutrons in Figs. 8 and 9 are presented in the spherical limit of the Nilsson basis for intuitive understanding of the shape staggering in a manner similar to the method in Ref. [30].

The topic of discussion that follows concerns the kink structure, which denotes a rapid increase in charge radii above a magic shell, observed across shell closures [37]. For example, recent data on Hg isotopes have shown a noticeable kink at $N = 126$ [30,41]. Moreover, a kink structure has been observed in K and Ca isotopes near the magic shell with $N = 20$
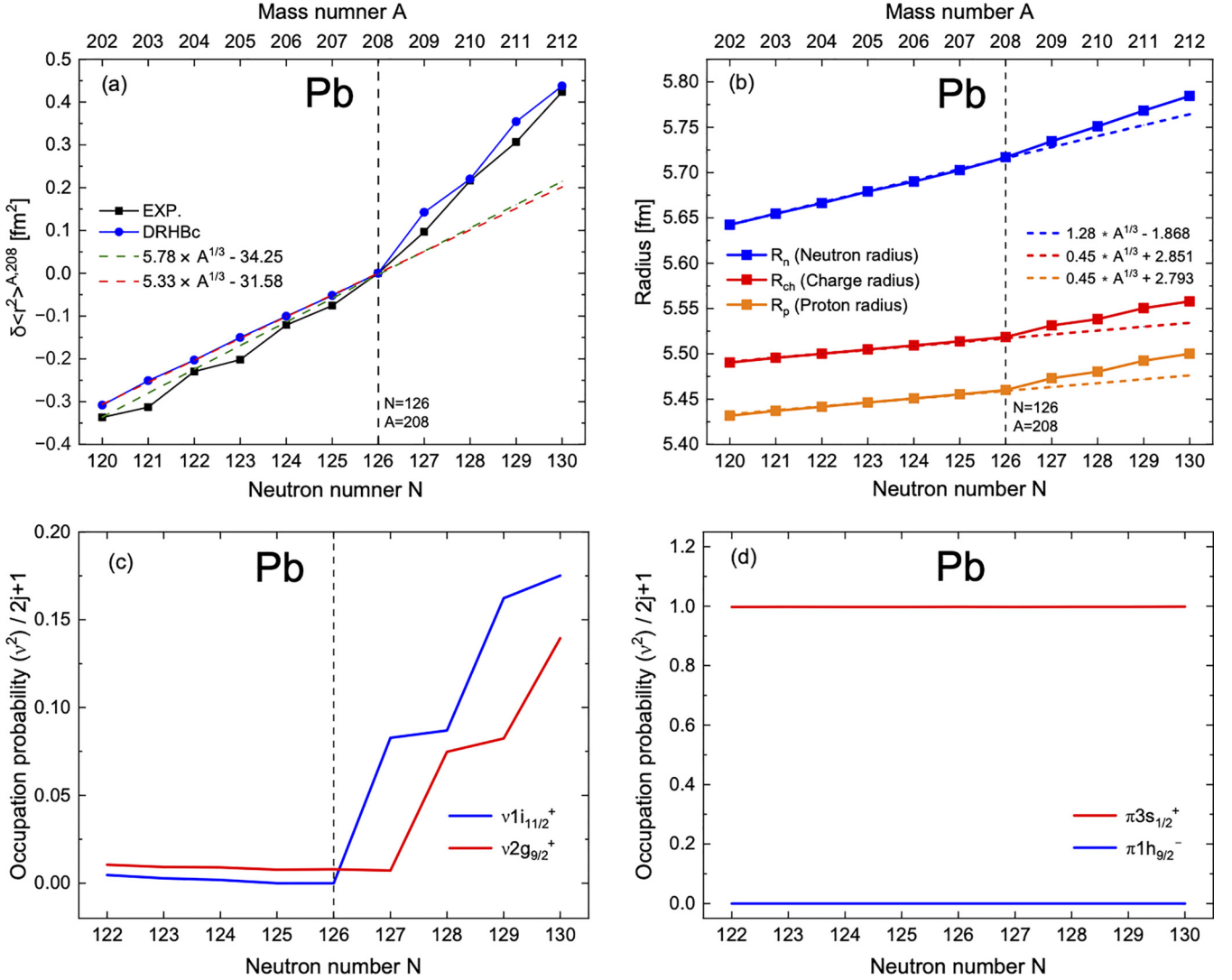
FIG. 10. Kink structure of Pb isotopes in the vicinity of $N = 126$ for the case normalized at ^{208}Pb isotope (a) and change of neutron, proton, and charge radii near ^{208}Pb. The dashed lines in (a) are just from the continuation of the data before the $N = 126$ case to show the kink structure, while the lines in (b) show how the radii deviate from the simple continuation. Panel (c) reveals a significant increase in the occupation probabilities of the $\nu 1i_{11/2}$ state compared to the $\nu 2g_{9/2}$ state. In panel (d), the occupation probabilities of proton states ($\pi 3s_{1/2}$ and $\pi 1h_{9/2}$) hardly ever change.

[38,42]. In our previous study [67], we demonstrated analogous patterns for Hg isotopes at the magic number $N = 126$. Furthermore, we observed analogous patterns for Pb isotopes beyond a different magic number, $N = 184$ [77].

In Fig. 10(a), our results for Pb isotopes exhibit a kink structure around the closed shell $N = 126$. Figure 10(b) illustrates the swelling of neutron radii leading to the kink structure from $N = 126$. Both results are compared to the trend lines denoted as dashed lines to show the kink structure. As mentioned in Refs. [67,113], pairing correlations cause the expansion of the neutron core, leading to an increase of the occupation probabilities for $\nu 2g_{9/2}$ and $\nu 1i_{11/2}$ states beyond the $N = 126$ closed shell [Fig. 10(c)]. In contrast, in Fig. 10(d), the occupation probabilities of proton states ($\pi 3s_{1/2}$ and $\pi 1h_{9/2}$) are hardly ever changed. This confirms that the kink structure is primarily caused by the swelling of neutrons, particularly of the $\nu 1i_{11/2}$ state, rather than by

the increase of the proton $\pi 3s_{1/2}$ and $\pi 1h_{9/2}$ states. Here we note that a Skyrme type interaction containing the isospin dependence of the spin-orbit term can also explain properly the kink structure in the Pb isotopes [114].

IV. SUMMARY AND CONCLUSION

We found that the shape coexistence is a key property to understand the interesting nuclear shape evolution. If we consider the shape coexistence of certain Au isotopes, we can certainly demonstrate two phenomena: (i) as we move from heavier to lighter masses, the $\delta \langle r^2 \rangle$ value increases significantly at $A = 186$, and (ii) the odd-even shape staggering of charge radii is clearly visible for ^{178}Au. Here, we adopt the oblate deformation of ^{176,177,179,187,188}Au because their TBEs by oblate deformation are about 1 MeV smaller than those by prolate deformation. However, other nuclei (up to ^{186}Au)

exhibit prolate shapes, because their local minima of TBEs for oblate deformation are 1 MeV larger than the minima for prolate deformation. Therefore, these prolate nuclei, which are excluded from the shape coexistence, do not exhibit significant change of charge radii. This implies that the odd-even shape staggering and the abrupt change could be a strong indicator of the shape coexistence of some Au isotopes, or vice versa. Here we note that possible existence of triaxial deformation [115] may lead the minima calculated in the present work to a saddle point in the (β, γ) plane [116]. We leave the possibility of the γ deformation in these isotopes as a future work.

Furthermore, within the DRHBc approach, we have successfully reproduced the kink structure of Pb observed around the $N = 126$ shell. This kink structure is caused by the increase in the occupation probabilities of $\nu 2g_{9/2}$ and $\nu 1i_{11/2}$ states beyond the closed shell at $N = 126$. The observed kink structure is closely linked to the swelling of the symmetric core at $N = 126$ followed by the pulling of the protons by the symmetry energy. We intend to further investigate the significant nuclear shape evolution and the kink structure of charge radii in K, Ca, and Bi isotopes near their magic shells using the DRHBc approach in future studies.

ACKNOWLEDGMENTS

[1] I. Angeli and K. P. Marinova, At. Data Nucl. Data Tables **99**, 69 (2013).

[2] I. Angeli and K. P. Marinova, J. Phys. G: Nucl. Part. Phys. **42**, 055108 (2015).

[3] N. Wang and T. Li, Phys. Rev. C **88**, 011301(R) (2013).

[4] C. Gorges, L. V. Rodríguez, D. L. Balabanski, M. L. Bissell, K. Blaum, B. Cheal, R. F. Garcia Ruiz, G. Georgiev, W. Gins, H. Heylen *et al.*, Phys. Rev. Lett. **122**, 192502 (2019).

[5] J. L. Wood, K. Heyde, W. Nazarewicz, M. Huyse, and P. van Duppen, Phys. Rep. **215**, 101 (1992).

[6] P. Cejnar, J. Jolie, and R. F. Casten, Rev. Mod. Phys. **82**, 2155 (2010).

[7] H. De Witte, A. N. Andreyev, N. Barre, M. Bender, T. E. Cocolios, S. Dean, D. Fedorov, V. N. Fedoseyev, L. M. Fraile, S. Franchoo *et al.*, Phys. Rev. Lett. **98**, 112502 (2007)

[8] K. T. Flanagan, K. M. Lynch, J. Billowes, M. L. Bissell, I. Budincevic, T. E. Cocolios, R. P. de Groote, S. De Schepper, V. N. Fedossev, S. Franchoo *et al.*, Phys. Rev. Lett. **111**, 212501 (2013).

[9] M. Bao and Q. Wei, Symmetry **13**, 2253 (2021).

[10] W. Geithner, T. Neff, G. Audi, K. Blaum, P. Delahaye, H. Feldmeier, S. George, C. Guénaut, F. Herfurth, A. Herlert *et al.*, Phys. Rev. Lett. **101**, 252502 (2008).

[11] W. Nörtershäuser, D. Tiedemann, M. Zákova, Z. Andjelkovic, K. Blaum, M. L. Bissell, R. Cazan, G. W. F. Drake, Ch. Geppert, M. Kowalska *et al.*, Phys. Rev. Lett. **102**, 062503 (2009).

[12] D. T. Yordanov, D. L. Balabanski, M. L. Bissell, K. Blaum, I. Budincevic, B. Cheal, K. Flanagan, N. Frömmgen, G. Georgiev, Ch. Geppert *et al.*, Phys. Rev. Lett. **116**, 032501 (2016).

[13] A. Bohr and B. R. Mottelson, *Nuclear Structure* (W. A. Benjamin, New York, 1975), Vol. 2.

[14] J. Duflo, Nucl. Phys. A **576**, 29 (1994).

[15] A. E. L. Dieperink and P. Van Isacker, Eur. Phys. J. A **42**, 269 (2009).

[16] Y. B. Qian, Z. Z. Ren, and D. D. Ni, Phys. Rev. C **89**, 024318 (2014).

[17] W. H. Ma, J. S. Wang, S. Mukherjee, Q. Wang, D. Patel, Y.-Y. Yang, J.-B. Ma, P. Ma, S.-L. Jin, Z. Ba *et al.*, Chin. Phys. C **41**, 044103 (2017).

[18] T. Li, Y. Luo, and N. Wang, At. Data Nucl. Data Tables **140**, 101440 (2021).

[19] S. Q. Zhang, J. Meng, S.-G. Zhou, and J. Y. Zeng, Eur. Phys. J. A **13**, 285 (2002).

[20] H. De Vries, C. De Jager, and C. De Vries, At. Data Nucl. Data Tables **36**, 495 (1987).

[21] M. Avgoulea, Y. P. Gangrsky, K. P. Marinova, S. G. Zemlyanoi, S. Fritzsche, D. Iablonskyi, C. Barbieri, E. C. Simpson, P. D. Stevenson, J. Billowes *et al.*, J. Phys. G: Nucl. Part. Phys. **38**, 025104 (2011).

[22] K. Marinova, J. Phys. Chem. Ref. Data **44**, 031214 (2015).

[23] I. Angeli and K. Marinova, J. Phys.: Conf. Ser. **724**, 012032 (2016).

[24] F. Boehm and P. L. Lee, At. Data Nucl. Data Tables **14**, 605 (1974).

[25] T. Manovitz, R. Shaniv, Y. Shapira, R. Ozeri, and N. Akerman, Phys. Rev. Lett. **123**, 203001 (2019).

[26] J. Z. Han, C. Pan, K. Y. Zhang, X. F. Yang, S. Q. Zhang, J. C. Berengut, S. Goriely, H. Wang, Y. M. Yu, J. Meng *et al.*, Phys. Rev. Res. **4**, 033049 (2022).

[27] A. Krieger, K. Blaum, M. L. Bissell, N. Frömmgen, Ch. Geppert, M. Hammen, K. Kreim, M. Kowalska, J. Krämer, T. Neff *et al.*, Phys. Rev. Lett. **108**, 142501 (2012).

[28] M. D. Seliverstov, T. E. Cocolios, W. Dexters, A. N. Andreyev, S. Antalic, A. E. Barzakh, B. Bastin, J. Büscher, I. G. Darby, D. V. Fedorov *et al.*, Phys. Lett. B **719**, 362 (2013).

[29] K. Minamisono, D. M. Rossi, R. Beerwerth, S. Fritzsche, D. Garand, A. Klose, Y. Liu, B. Maaß, P. F. Mantica, A. J. Miller *et al.*, Phys. Rev. Lett. **117**, 252501 (2016).

[30] B. A. Marsh, T. Day Goodacre, S. Sels, Y. Tsunoda, B. Andel, A. N. Andreyev, N. A. Althubiti, D. Atanasov, A. E. Barzakh, J. Billowes *et al.*, Nat. Phys. **14**, 1163 (2018).

[31] S. Kaufmann, J. Simonis, S. Bacca, J. Billowes, M. L. Bissell, K. Blaum, B. Cheal, R. F. Garcia Ruiz, W. Gins, C. Gorges *et al.*, Phys. Rev. Lett. **124**, 132502 (2020).

[32] A. J. Miller, K. Minamisono, A. Klose, D. Garand, C. Kujawa, J. D. Lantis, Y. Liu, B. Maaß, P. F. Mantica, W. Nazarewicz *et al.*, Nat. Phys. **15**, 432 (2019).

[33] R. F. Garcia Ruiz, M. L. Bissell, K. Blaum, A. Ekstrm, N. Frömmgen, G. Hagen, M. Hammen, K. Hebeler, J. D. Holt, G. R. Jansen *et al.*, Nat. Phys. **12**, 594 (2016).

[34] R. P. de Groote, J. Billowes, C. L. Binnersley, M. L. Bissell, T. E. Cocolios, T. Day Goodacre, G. J. Farooq-Smith, D. V. Fedorov, K. T. Flanagan, S. Franchoo *et al.*, Nat. Phys. **16**, 620 (2020).

[35] J. G. Cubiss, A. N. Andreyev, A. E. Barzakh, P. Van Duppen, S. Hilaire, S. Péru, S. Goriely, M. Al Monthery, N. A. Althubiti, B. Andel *et al.*, Phys. Rev. Lett. **131**, 202501 (2023).

[36] M. Rosenbusch, P. Ascher, D. Atanasov, C. Barbieri, D. Beck, K. Blaum *et al.*, Phys. Rev. Lett. **114**, 202501 (2015).

[37] K. Kreim, M. Bissell, J. Papuga, K. Blaum, M. De Rydt, R. F. Garcia Ruiz, Ch. Borgmann, M. Breitenfeldt, R. B. Cakirli, A. Cipollone *et al.*, Phys. Lett. B **731**, 97 (2014).

[38] Á. Koszorús, X. F. Yang, J. Billowes, C. L. Binnersley, M. L. Bissell, T. E. Cocolios, G. J. Farooq-Smith, R. P. de Groote, K. T. Flanagan, S. Franchoo *et al.*, Phys. Rev. C **100**, 034304 (2019).

[39] Á. Koszorús, X. F. Yang, W. G. Jiang, S. J. Novario, S. W. Bai, J. Billowes, C. L. Binnersley, M. L. Bissell, T. E. Cocolios, B. S. Cooper *et al.*, Nat. Phys. **17**, 439 (2021); **17**, 539(E) (2021).

[40] S. Geldhof, M. Kortelainen, O. Beliuskina, P. Campbell, L. Caceres, L. Cañete, B. Cheal, K. Chrysalidis, C. S. Devlin, R. P. de Groote *et al.*, Phys. Rev. Lett. **128**, 152501 (2022).

[41] T. Day Goodacre, A. V. Afanasjev, A. E. Barzakh, B. A. Marsh, S. Sels, P. Ring, H. Nakada, A. N. Andreyev, P. Van Duppen, N. A. Althubiti *et al.*, Phys. Rev. Lett. **126**, 032502 (2021).

[42] M. Tanaka, M. Takechi, M. Fukuda, D. Nishimura, T. Suzuki, Y. Tanaka, T. Moriguchi, D. S. Ahn, A. Aimaganbetov, M. Amano *et al.*, Phys. Rev. Lett. **124**, 102501 (2020).

[43] F. Wienholtz, D. Beck, K. Blaum, Ch. Borgmann, M. Breitenfeldt, R. B. Cakirli, S. George, F. Herfurth, J. D. Holt, M. Kowalska *et al.*, Nature (London) **498**, 346 (2013).

[44] T. Kühl, P. Dabkiewicz, C. Duke, H. Fischer, H.-J. Kluge, H. Kremmling, and E.-W. Otten, Phys. Rev. Lett. **39**, 180 (1977).

[45] G. Ulm, S. K. Bhattacherjee, P. Dabkiewicz, G. Huber, H. -J. Kluge, T. Kühl, H. Lochmann, E. -W. Otten, K. Wendt, S. A. Ahmad *et al.*, Z. Phys. A **325**, 247 (1986).

[46] M. Anselment, W. Faubel, S. Goering, A. Hanser, G. Meisel, H. Rebel, and G. Schatz, Nucl. Phys. A **451**, 471 (1986).

[47] A. Barzakh, A. N. Andreyev, C. Raison, J. G. Cubiss, P. Van Duppen, S. Péru, S. Hilaire, S. Goriely, B. Andel, S. Antalic *et al.*, Phys. Rev. Lett. **127**, 192501 (2021).

[48] P. M. Goddard, P. D. Stevenson, and A. Rios, Phys. Rev. Lett. **110**, 032503 (2013).

[49] M. Hammen, W. Nörtershäuser, D. L. Balabanski, M.L. Bissell, K. Blaum, I. Budinčević, B. Cheal, K.T. Flanagan, N. Frömmgen, G. Georgiev *et al.*, Phys. Rev. Lett. **121**, 102501 (2018).

[50] M. Reponen, R. P. de Groote, L. Al Ayoubi, O. Beliuskina, M. L. Bissell, P. Campbell, L. Cañete, B. Cheal, K. Chrysalidis, C. Delafosse *et al.*, Nat. Commun. **12**, 4596 (2021).

[51] S. Malbrunot-Ettenauer, S. Kaufmann, S. Bacca, C. Barbieri, J. Billowes, M. L. Bissell, K. Blaum, B. Cheal, T. Duguet, R. F. Garcia Ruiz *et al.*, Phys. Rev. Lett. **128**, 022502 (2022).

[52] B. H. Sun, C. Y. Liu, and H. X. Wang, Phys. Rev. C **95**, 014307 (2017).

[53] C. Ma, Y. Y. Zong, Y. M. Zhao, and A. Arima, Phys. Rev. C **104**, 014303 (2021).

[54] F. Buchinger and J. M. Pearson, Phys. Rev. C **72**, 057305 (2005).

[55] H. Iimura and F. Buchinger, Phys. Rev. C **78**, 067301 (2008).

[56] S. Goriely, N. Chamel, and J. M. Pearson, Phys. Rev. C **82**, 035804 (2010).

[57] P.-G. Reinhard and W. Nazarewicz, Phys. Rev. C **95**, 064328 (2017).

[58] K. Zhang, M.-K. Cheoun, Y.-B. Choi, P. S. Chong, J. Dong, Z. Dong, X. Du, L. Geng, Eunja Ha, X.-T. He *et al.*, At. Data Nucl. Data Tables **144**, 101488 (2022).

[59] X. W. Xia, Y. Lim, P. W. Zhao, H. Z. Liang, X. Y. Qu, Y. Chen, H. Liu, L. F. Zhang, S. Q. Zhang, Y. Kim *et al.*, At. Data Nucl. Data Tables **121-122**, 1 (2018).

[60] U. C. Perera, A. V. Afanasjev, and P. Ring, Phys. Rev. C **104**, 064313 (2021).

[61] C. Forssén, E. Caurier, and P. Navrátil, Phys. Rev. C **79**, 021303(R) (2009).

[62] P. Choudhary, P. C. Srivastava, and P. Navrátil, Phys. Rev. C **102**, 044309 (2020).

[63] Y. Ma, C. Su, J. Liu, Z. Ren, C. Xu, and Y. Gao, Phys. Rev. C **101**, 014304 (2020).

[64] D. Wu, C. L. Bai, H. Sagawa, and H. Q. Zhang, Phys. Rev. C **102**, 054323 (2020).

[65] J. Q. Ma and Z. H. Zhang, Chin. Phys. C **46**, 074105 (2022).

[66] X.-X. Dong, R. An, J.-X. Lu, and L.-S. Geng, Phys. Lett. B **838**, 137726 (2023).

[67] Myeong-Hwan Mun, Seonghyun Kim Myung-Ki Cheoun, W. Y. So, S. Choi, and E. Ha, Phys. Lett. B **847**, 138298 (2023)

[68] S. Sels, T. Day Goodacre, B. A. Marsh, A. Pastore, W. Ryssens, Y. Tsunoda, N. Althubiti, B. Andel, A. N. Andreyev, D. Atanasov *et al.*, Phys. Rev. C **99**, 044306 (2019).

[69] S.-G. Zhou, J. Meng, P. Ring, and E.-G. Zhao, Phys. Rev. C **82**, 011301(R) (2010).

[70] L. Li, J. Meng, P. Ring, E.-G. Zhao, and S.-G. Zhou, Phys. Rev. C **85**, 024312 (2012).

[71] L.-L. Li, J. Meng, P. Ring, E.-G. Zhao, and S.-G. Zhou, Chin. Phys. Lett. **29**, 042101 (2012).

[72] K. Zhang, M.-K. Cheoun, Y.-B. Choi, P. S. Chong, J. Dong, L. Geng, E. Ha, X. He, C. Heo, M. C. Ho *et al.* (DRHBc Mass Table Collaboration), Phys. Rev. C **102**, 024314 (2020).

[73] C. Pan, M.-K. Cheoun, Y.-B. Choi, J. Dong, X. Du, X.-H. Fan, W. Gao, L. Geng, E. Ha, X.-T. He *et al.* (DRHBc Mass Table Collaboration), Phys. Rev. C **106**, 014316 (2022).

[74] K. Zhang, X. He, J. Meng, C. Pan, C. Shen, C. Wang, and S. Zhang, Phys. Rev. C **104**, L021301 (2021).

[75] C. Pan, K. Y. Zhang, P. S. Chong, C. Heo, M. C. Ho, J. Lee, Z. P. Li, W. Sun, C. K. Tam, S. H. Wong *et al.*, Phys. Rev. C **104**, 024331 (2021).

[76] P. Guo, X. Cao, K. Chen, Z. Chen, M.-K. Cheoun, Y.-B. Choi *et al.*, At. Data Nucl. Data Tables **158**, 101661 (2024).

[77] S. Kim, M.-H. Mun, M.-K. Cheoun, and E. Ha, Phys. Rev. C **105**, 034340 (2022).

[78] C. Pan, K. Zhang, and S. Zhang, Int. J. Mod. Phys. E **28**, 1950082 (2019).

[79] E. J. In, P. Papakonstantinou, Y. Kim, and S.-W. Hong, Int. J. Mod. Phys. E **30**, 2150009 (2021).

[80] X.-X. Sun, Phys. Rev. C **103**, 054315 (2021).

[81] X.-X. Sun and S.-G. Zhou, Sci. Bull. **66**, 2072 (2021).

[82] X.-X. Sun and S.-G. Zhou, Phys. Rev. C **104**, 064319 (2021).

[83] X.-X. Sun, J. Zhao, and S.-G. Zhou, Nucl. Phys. A **1003**, 122011 (2020).

[84] X.-X. Sun, J. Zhao, and S.-G. Zhou, Phys. Lett. B **785**, 530 (2018).

[85] Z. H. Yang, Y. Kubota, A. Corsi, K. Yoshida, X.-X. Sun, J. G. Li, M. Kimura, N. Michel, K. Ogata, C. X. Yuan *et al.*, Phys. Rev. Lett. **126**, 082501 (2021).

[86] K. Y. Zhang, D. Y. Wang, and S. Q. Zhang, Phys. Rev. C **100**, 034312 (2019)

[87] K. Y. Zhang, P. Papakonstantinou, M.-H. Mun, Y. Kim, H. Yan, and X.-X. Sun, Phys. Rev. C **107**, L041303 (2023)

[88] K. Y. Zhang, S. Q. Yang, J. L. An, S. S. Zhang, P. Papakonstantinou, M.-H. Mun, Y. Kim, and H. Yan, Phys. Lett. B **844**, 138112 (2023)

[89] J.-L. An, K.-Y. Zhang, Q. Lu, S.-Y. Zhong, and S.-S. Zhang, Phys. Lett. B **849**, 138422 (2024).

[90] P. Guo, C. Pan, Y. C. Zhao, X. K. Du, and S. Q. Zhang, Phys. Rev. C **108**, 014319 (2023).

[91] H. Kucharek and P. Ring, Z. Phys. A **339**, 23 (1991).

[92] S.-G. Zhou, J. Meng, and P. Ring, Phys. Rev. C **68**, 034323 (2003).

[93] K. Y. Zhang, C. Pan, and S. Q. Zhang, Phys. Rev. C **106**, 024302 (2022).

[94] P. Ring and P. Schuck, *The Nuclear Many-Body Problem* (Springer, Berlin, 2004).

[95] C. E. Price and G. E. Walker, Phys. Rev. C **36**, 354 (1987).

[96] Y. Xiang, Q. Luo, S. Yang, and K. Zhang, Symmetry **15**, 1420 (2023).

[97] S. Perez-Martin and L. M. Robledo, Phys. Rev. C **78**, 014304 (2008).

[98] C. Pan, K. Zhang, and S. Zhang, Phys. Lett. B **855**, 138792 (2024).

[99] M. Wang, W. J. Huang, F. G. Kondev, G. Audi, and S. Naimi, Chin. Phys. C **45**, 030003 (2021).

[100] NNDC (National Nuclear Data Center), Brookhaven National Laboratory, https://www.nndc.bnl.gov/nudat2/

[101] J. L. Wood and K. Heyde, J. Phys. G: Nucl. Part. Phys. **43**, 020402 (2016).

[102] A. Gade and S. N. Liddick, J. Phys. G: Nucl. Part. Phys. **43**, 024001 (2016).

[103] K. Heyde and J. L. Wood, Rev. Mod. Phys. **83**, 1467 (2011); **83**, 1655(E) (2011).

[104] E. Nácher, A. Algora, B. Rubio, J. L. Taín, D. Cano-Ott, S. Courtin, Ph. Dessagne, F. Maréchal, Ch. Miehé, E. Poirier *et al.*, Phys. Rev. Lett. **92**, 232501 (2004).

[105] A. N. Andreyev, M. Huyse, P. Van Duppen, L. Weissman, D. Ackermann, J. Gerl, F. P. Hessberger, S. Hofmann, A. Kleinböhl, G. Münzenberg *et al.*, Nature (London) **405**, 430 (2000).

[106] J. Ojala, J. Pakarinen, P. Papadakis, J. Sorri, M. Sandzelius, D. M. Cox, K. Auranen, H. Badran, P. J. Davies, T. Grahn *et al.*, Commun. Phys. **5**, 213 (2022).

[107] P. F. Mantica, Physics **2**, 18 (2009).

[108] G. Savard, J. E. Crawford, J. K. P. Lee, G. Thekkadath, H. T. Duong, J. Pinard, F. Le Blanc, P. Kilcher, J. Obert, J. Oms *et al.* (The ISOCELE Collaboration), Nucl. Phys. A **512**, 241 (1990).

[109] G. Passler, J. Rikovska, E. Arnold, H.-J. Kluge, L. Monz, R. Neugart, H. Ravn, and K. Wendt (ISOLDE Collaboration), Nucl. Phys. A **580**, 173 (1994).

[110] F. Le Blanc, J. Obert, J. Oms, J. C. Putaux, B. Roussiére, J. Sauvage, J. Pinard, L. Cabaret, H. T. Duong, G. Huber *et al.* (ISOLDE Collaboration), Phys. Rev. Lett. **79**, 2213 (1997).

[111] M. D. Seliverstov, A. N. Andreyev, N. Barré, A. E. Barzakh, S. Dean, H. De Witte, D. V. Fedorov, V. N. Fedoseyev, L. M. Fraile, S. Franchoo *et al.*, Eur. Phys. J. A **41**, 315 (2009).

[112] B. Pritychenko, M. Birch, B. Singh, and M. Horoi, At. Data Nucl. Data Tables **107**, 1 (2016).

[113] W. Horiuchi and T. Inakura, Phys. Rev. C **105**, 044303 (2022); **101**, 061301(R) (2020).

[114] M. M. Sharma, G. Lalazissis, J. Konig, and P. Ring, Phys. Rev. Lett. **74**, 3744 (1995).

[115] K. Y. Zhang, S. Q. Zhang, and J. Meng, Phys. Rev. C **108**, L041301 (2023).

[116] Y. L. Yang, Y. K. Wang, P. W. Zhao, and Z. P. Li, Phys. Rev. C **104**, 054312 (2021).